International Journal of Control

ISSN: (Print) (Online) Journal homepage: www.tandfonline.com/journals/tcon20

Static anti-windup compensator design for autonomous guidance and control of quadrotors*

Majid Shahbazzadeh & Christopher M. Richards

INTERNATIONAL JOURNAL OF CONTROL
https://doi.org/10.1080/00207179.2025.2454910

Static anti-windup compensator design for autonomous guidance and control of quadrotors*

Majid Shahbazzadeh and Christopher M. Richards

Department of Mechanical Engineering, University of Louisville, Louisville, KY, USA

ABSTRACT
In this paper, the problem of anti-windup compensator (AWC) design for implementation in the autonomous guidance and control of quadrotors is addressed. The flight environment contains obstacles with no prior knowledge of their locations. Instead, obstacles location are determined in real time, and the locations are used by a guidance algorithm for avoidance. Wind disturbances are also considered since their presence can potentially result in saturation of the propellers. When this occurs, the flight can become unstable, leading to a crash. Designing an AWC to mitigate the effects of saturation in the control system of a quadrotor can be a challenging task due to the heavy couplings and complex nonlinear dynamics. For this reason, we propose a new structure to design a static AWC-based control system to solve this problem. The effectiveness of the proposed theoretical results are verified by comparing results from simulation experiments.

ARTICLE HISTORY
Received 1 March 2024
Accepted 12 January 2025

KEYWORDS
Anti-windup compensation; guidance; control; quadrotors

1. Introduction

Quadrotor unmanned aerial vehicles (UAVs) have been extensively studied and utilised due to their simple structure and vertical take-off and landing capabilities (Jeon et al., 2020; Lu & Xing, 2022; Yang et al., 2020). These unique features make quadrotors versatile for various applications, ranging from recreational drones to professional use in industries such as cinematography, agriculture, surveillance, and search and rescue operations (Sabour et al., 2023).

UAVs, along with various other physical control systems, encounter constraints in both magnitude and/or rate, where an output greater than what the actuator can deliver may be demanded by the system's controller. This phenomenon is referred to as actuator saturation, which significantly affects the flight quality (Chang et al., 2023). When actuator saturation occurs, the UAV's control response may degrade, affecting its stability, and potentially leading to a crash. Some studies offer *ad hoc* solutions, where the control law and actuator requirements of the system are pre-designed to mitigate the tendency of the system to saturate. However, these solutions that mitigate saturation are not effective when controller response to large exogenous inputs results in the need for large control signals.

Designing an anti-windup compensator (AWC) is an effective approach to alleviate the effects from actuator saturation (Huang et al., 2022). Generally, in anti-windup compensation, a linear controller is initially designed without explicit consideration of the saturation constraints. Subsequently, an AWC is designed to handle the saturation constraints. In fact, the AWC is designed to guarantee that stability is maintained and that less performance degradation occurs compared to when no anti-windup is employed (Tarbouriech et al., 2011). In recent years, many studies have focussed on AWC design for quadrotors (Buratti et al., 2019; Falkenberg et al., 2012; Ghignoni et al., 2020; Ofodile & Turner, 2016, 2017; Ofodile et al., 2015).

On the other hand, while the AWC is typically constructed from a linear (or linearised) model of plant's dynamics (Galeani et al., 2009; Tarbouriech et al., 2011; Tarbouriech & Turner, 2009; Turner et al., 2007; Zaccarian & Teel, 2011), this approach is inadequate for a multi-loop guidance and control architecture for a quadrotor such as that presented in Kirven and Hoagg (2021). More precisely, although some recent work on attitude only control has been successfully applied to the linearised attitude dynamics about the hover operating point (Farber & Richards, 2024; Richards & Turner, 2020), linearisation of the dynamics about the hover operating point fails to provide a sufficient representation of the dynamics, especially during aggressive maneuvers and/or when wind disturbances occur. Therefore, the full nonlinear vehicle dynamics are necessary for the design of an AWC-based guidance and control system for quadrotors under these circumstances, which motivates this study.

In this paper, we present an integrated autonomous guidance and AWC-based control method for a quadrotor operating in an environment with obstacles whose locations are unknown, but measured in real-time during flight. Generally, designing an AWC for quadrotors is difficult due to the highly coupled nonlinear dynamics of the vehicle. This challenge is overcome through a novel reformulation of the saturation constraints so that the full nonlinear dynamics of quadrotors can be used in an anti-windup control design scheme. This problem is converted to a set of linear matrix inequality conditions so that by solving

CONTACT Christopher M. Richards chris.richards@louisville.edu Department of Mechanical Engineering, University of Louisville, Louisville, KY 40292, USA

* A preliminary version of this paper was presented at the 2024 American Control Conference.

them, the controller and AWC gains are designed simultaneously. Simulation results are presented for three cases: 1-without saturation, 2-with saturation and without AWC, 3-with saturation and with AWC. The results show the effectiveness and advantages of the proposed anti-windup method.

The main contributions of this article are as follows:

- An AWC-based controller is designed for a quadrotor to track the desired signals from a guidance algorithm.
- To design the AWC-based controller, the full nonlinear dynamics are employed, as the linearisation technique may fail to provide a sufficient representation of the dynamics.
- The problem of determining the controller and AWC gains are converted to a set of linear matrix inequalities despite the complex nonlinear dynamics of the vehicle.
- The novel reformulation of the saturation constraints presented in this article has the potential to be extended to various other constrained systems.

The paper is arranged as follows. The problem formulation is provided in Section 2. The main results are given in Section 3. The simulation results are presented in Section 4. Finally, a conclusion is drawn in Section 5.

2. Problem formulation

First, we present the basic definitions that are needed in the sequel.

Definition 2.1: The saturation function $\mathrm{sat}(\cdot):\mathbb{R}^m \to \mathbb{R}^m$ is defined as

$$\mathrm{sat}(u_i)_{\underline{u}_i}^{\overline{u}_i} = \begin{cases} \overline{u}_i & \overline{u}_i < u_i, \\ u_i & \underline{u}_i \le u_i \le \overline{u}_i, \qquad i = 1, \cdots, m \\ \underline{u}_i & u_i < \underline{u}_i, \end{cases} \tag{1}$$

where $\overline{u}_i$ and $\underline{u}_i$ are, respectively, the upper and lower saturation limits of the ith row of u.

Definition 2.2: The deadzone function $\mathrm{Dz}(\cdot):\mathbb{R}^m \to \mathbb{R}^m$ is defined as

$$\mathrm{Dz}_{\underline{u}_i}^{\overline{u}_i}(u_i) := u_i - \mathrm{sat}_{\underline{u}_i}^{\overline{u}_i}(u_i). \tag{2}$$

The inertial and body frames are illustrated in Figure 1. Consider I as the inertial frame. The origin (o_I) of this frame is arbitrarily chosen on the Earth's surface, with orthogonal unit vectors $\hat{\imath}, \hat{\jmath}$, and $\hat{k}$. Let B represent the body frame, attached to the quadrotor's centre of mass (o_B), with orthogonal unit vectors $\hat{b}_1, \hat{b}_2$, and $\hat{b}_3$. The position of o_B relative to o_I is $q = x\hat{\imath} + y\hat{\jmath} + z\hat{k}$.

The rotation matrix from the inertial frame to the body frame is

$$\mathcal{O} = \begin{bmatrix} c_\theta c_\psi & c_\theta s_\psi & -s_\theta \\ s_\phi s_\theta c_\psi - c_\phi s_\psi & s_\phi s_\theta s_\psi + c_\phi c_\psi & s_\phi c_\theta \\ c_\phi s_\theta c_\psi + s_\phi s_\psi & c_\phi s_\theta s_\psi - s_\phi c_\psi & c_\phi c_\theta \end{bmatrix}, \tag{3}$$

where ϕ, θ, and ψ are the Euler angles, $s_\delta = \sin\delta$, and $c_\delta = \cos\delta$.

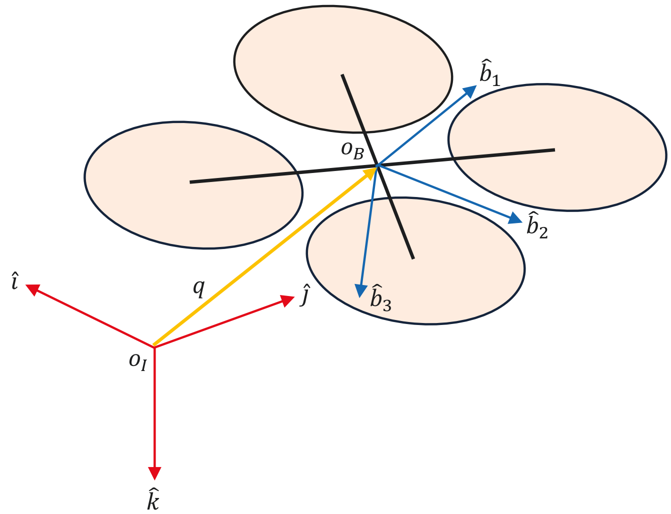

Figure 1. Inertial and body frames.

The thrust vector is $-T\hat{b}_3$, where

$$T = k\sum_{i=0}^{4} \varpi_i{}^2, \tag{4}$$

k is the propeller thrust constant, and $\varpi_i > 0$ is the angular speed of the ith propeller. From (4), it is obvious that the minimum value of the thrust force is zero, i.e. $\underline{T} = 0$.

The translational dynamics of a quadrotor with constrained thrust in the inertial frame can be expressed as

$$\begin{aligned} \ddot{x} &= -\mathrm{sat}_{\underline{T}}^{\overline{T}}(T)\left(c_\phi s_\theta c_\psi + s_\phi s_\psi\right)/m, \\ \ddot{y} &= -\mathrm{sat}_{\underline{T}}^{\overline{T}}(T)\left(c_\phi s_\theta s_\psi - s_\phi c_\psi\right)/m, \\ \ddot{z} &= g - \mathrm{sat}_{\underline{T}}^{\overline{T}}(T) c_\phi c_\theta/m, \end{aligned} \tag{5}$$

where m is the mass of the vehicle and g is the gravitational constant.

The rotational dynamics of a quadrotor with constrained body torques in the body frame can be described by

$$J\dot{\omega} + \omega \times J\omega = \mathrm{sat}_{\underline{\tau}}^{\overline{\tau}}(\tau), \tag{6}$$

where $\omega = [\omega_1, \omega_2, \omega_3]'$ is the angular velocity vector of the quadrotor with respect to the body frame, J is the inertia matrix, and τ is the control torque vector given as

$$\tau = \tau_1\hat{b}_1 + \tau_2\hat{b}_2 + \tau_3\hat{b}_3, \tag{7}$$

where

$$\begin{aligned} \tau_1 &= kl\left(\varpi_1^2 - \varpi_2^2 - \varpi_3^2 + \varpi_4^2\right), \\ \tau_2 &= kl\left(\varpi_1^2 + \varpi_2^2 - \varpi_3^2 - \varpi_4^2\right), \\ \tau_3 &= b\left(\varpi_1^2 - \varpi_2^2 + \varpi_3^2 - \varpi_4^2\right), \end{aligned}$$

and l and b are the thrust moment arm and the propeller drag constant, respectively.

The vector ω can be expressed as

$$\omega = Q\dot{\Gamma}, \tag{8}$$

where

$$Q = \begin{bmatrix} 1 & 0 & -s_\theta \\ 0 & c_\phi & s_\phi c_\theta \\ 0 & -s_\phi & c_\phi c_\theta \end{bmatrix}, \quad \Gamma = \begin{bmatrix} \phi \\ \theta \\ \psi \end{bmatrix}. \tag{9}$$

For all $\theta \neq \pm\pi/2$, the vector $\dot{\Gamma}$ can be obtained as

$$\dot{\Gamma} = Q^{-1}\omega. \tag{10}$$

The AWC-based attitude controller is constructed as follows:

$$\tau = \tau_\beta + \tau_C + \tau_A, \tag{11}$$

where

$$\tau_\beta = J\dot{\omega}_d + \omega_d \times J\omega, \quad \tau_C = -K_\omega e_\omega,$$
$$\tau_A = -K_a \mathrm{Dz}_{\underline{\tau}-\tau_\beta}^{\overline{\tau}-\tau_\beta}(\tau_C + \tau_A),$$

K_ω, K_a are the controller and AWC gains, respectively, and $e_\omega := \omega - \omega_d$, where ω_d is the desired angular velocity.

In addition, the AWC-based velocity controller is considered as

$$T = T_\beta + T_C + T_A, \tag{12}$$

where

$$T_\beta = \frac{m(g - \dot{\mathcal{W}}_d)}{c_\phi c_\theta}, \quad T_C = \frac{m}{c_\phi c_\theta} K_{\mathcal{W}} e_{\mathcal{W}},$$
$$T_A = -K_{\bar{a}} \mathrm{Dz}_{\underline{T}-T_\beta}^{\overline{T}-T_\beta}(T_C + T_A),$$

and $K_{\mathcal{W}}, K_{\bar{a}}$ are the controller and AWC gains, respectively. In addition, $e_{\mathcal{W}} := \mathcal{W} - \mathcal{W}_d$, where $\mathcal{W} = \dot{z}$ and $\mathcal{W}_d = \dot{z}_d$ is the desired translational velocity in the z-direction.

The following assumptions are considered to obtain the main results.

Assumption 2.1: *It is assumed that for all $t \geq 0$, $\phi(t) \in (-\pi/2, \pi/2)$ and $\theta(t) \in (-\pi/2, \pi/2)$. The range of the roll and pitch angles (ϕ, θ) for a quadrotor depend on its specific design and flight control system, as well as its intended use. However, for typical quadrotor flight, the roll and pitch angles (ϕ, θ) are usually within $(-\pi/2, \pi/2)$.*

Assumption 2.2: *In this paper, it is assumed that*

$$|(J\dot{\omega}_d + \omega_d \times J\omega)_i| \leq \overline{\tau}_i, \tag{13}$$

where $(\cdot)_i$ indicates the ith row of the vector within parentheses. The saturation bounds for the control torques are considered symmetric (i.e. $\overline{\tau} = -\underline{\tau}$) and would be for quadrotors with identical propellers and rotors.

For small consumer drones, the inertia values are typically relatively low due to their lightweight and compact design. Therefore, the value of the expression inside $|\cdot|$ in (13) is generally small.

Assumption 2.3: *In this paper, we assume that*

$$\underline{T} \leq \frac{m}{c_\phi c_\theta}(g - \dot{\mathcal{W}}_d) \leq \overline{T}. \tag{14}$$

Remark 2.1: For the main results, it is not necessary that conditions (13) and (14) are satisfied for all $t \geq 0$. In fact, it is enough that these conditions are satisfied for all $t \geq t_1$, where $t_1 \geq 0$ is a finite time.

We introduce the following lemma that is required to prove the theorems.

Lemma 2.1: *Given that the vectors $\nu_a, \nu_b \in \mathbb{R}^n$ and a positive diagonal matrix $\mathscr{W} = \mathrm{diag}(\mathscr{W}_{11}, \ldots, \mathscr{W}_{nn})$. The following sector condition is satisfied if $\underline{\nu}_i \leq \nu_{ai} \leq \overline{\nu}_i$ and $\underline{\nu}_i \leq 0 \leq \overline{\nu}_i$ for $i = \{1, \ldots, n\}$:*

$$\mathrm{sat}_{\underline{\nu}-\nu_a}^{\overline{\nu}-\nu_a}(\nu_b)' \mathscr{W} \mathrm{Dz}_{\underline{\nu}-\nu_a}^{\overline{\nu}-\nu_a}(\nu_b) \geq 0. \tag{15}$$

Proof of Lemma: Since $\mathscr{W}$ is a diagonal matrix, condition (15) can be rewritten as

$$\sum_{i=1}^{n} \mathrm{sat}_{\underline{\nu}_i-\nu_{ai}}^{\overline{\nu}_i-\nu_{ai}}(\nu_{bi}) \mathscr{W}_{ii} \mathrm{Dz}_{\underline{\nu}_i-\nu_{ai}}^{\overline{\nu}_i-\nu_{ai}}(\nu_{bi}) \geq 0. \tag{16}$$

Let us consider the following cases:

(1) $\overline{\nu}_i - \nu_{ai} < \nu_{bi}$:
In this case, we have:

$$\begin{aligned} \mathrm{sat}_{\underline{\nu}_i-\nu_{ai}}^{\overline{\nu}_i-\nu_{ai}}(\nu_{bi}) &= \overline{\nu}_i - \nu_{ai} > 0, \\ \mathrm{Dz}_{\underline{\nu}_i-\nu_{ai}}^{\overline{\nu}_i-\nu_{ai}}(\nu_{bi}) &= \nu_{ai} + \nu_{bi} - \overline{\nu}_i > 0. \end{aligned} \tag{17}$$

(2) $\underline{\nu}_i - \nu_{ai} \leq \nu_{bi} \leq \overline{\nu}_i - \nu_{ai}$:
This case leads to:

$$\mathrm{sat}_{\underline{\nu}_i-\nu_{ai}}^{\overline{\nu}_i-\nu_{ai}}(\nu_{bi}) = \nu_{bi}, \quad \mathrm{Dz}_{\underline{\nu}_i-\nu_{ai}}^{\overline{\nu}_i-\nu_{ai}}(\nu_{bi}) = 0. \tag{18}$$

(3) $\nu_{bi} < \underline{\nu}_i - \nu_{ai}$:
In this case, one can obtain:

$$\begin{aligned} \mathrm{sat}_{\underline{\nu}_i-\nu_{ai}}^{\overline{\nu}_i-\nu_{ai}}(\nu_{bi}) &= \underline{\nu}_i - \nu_{ai} < 0, \\ \mathrm{Dz}_{\underline{\nu}_i-\nu_{ai}}^{\overline{\nu}_i-\nu_{ai}}(\nu_{bi}) &= \nu_{ai} + \nu_{bi} - \underline{\nu}_i < 0. \end{aligned} \tag{19}$$

All the above three cases imply that the condition (15) is satisfied. ■

3. Main results

This section is devoted to an integrated control and guidance approach for a quadrotor to avoid obstacles and reach a desired destination while accounting for input saturation. A full schematic of the proposed approach, which is based upon the work of Kirven and Hoagg (2021), is illustrated in Figure 2. The control approach operates as follows. The yellow box shows that the guidance algorithm outputs the velocity commands Σ_c by using the obstacle locations, which can be provided by an onboard sensor, along with the destination point and current position, obtained through integration of the vehicle's translational velocities Σ. The magenta box indicates that the velocity commands Σ_c provided by the guidance algorithm are passed through low pass filters (58), which lead to the desired velocities Σ_d and their derivatives $\dot{\Sigma}_d$. The desired Euler angles $\Gamma_d =$

$[\phi_d, \theta_d, \psi_d]'$ and desired angular velocities ω_d are obtained in the green boxes. Note that ψ_d is the desired yaw of the vehicle, which would be provided by the guidance algorithm if it were necessary to rotate the vehicle to detect objects. In this study, we assume that this is not necessary. Therefore, $\psi_d = 0$ throughout. In the purple boxes, the velocity and attitude controllers generate the nominal control thrust signals (T_β, T_C) and nominal control torque signals (τ_β, τ_C). Finally, the red and blue boxes illustrate the proposed AWC method for the translational and rotational dynamics, respectively.

3.1 AWC-based control

The coupled and nonlinear dynamics of a quadrotor introduce challenges into the stability analysis and design of the controller and AWC. This is further complicated by the fact that we also deal with the tracking desired signals, which requires the term τ_β in the AWC-based attitude controller (11), and T_β in the AWC-based velocity controller (12). In general, tracking problems are more challenging compared to stabilisation problems, especially for nonlinear systems (Liu et al., 2014; Tseng et al., 2001). Moreover, they become significantly more difficult when control signals are subject to saturation. To resolve this problem, we propose a saturation function with modified limits so that τ_β does not directly participate as an input to the saturation function $\text{sat}(\cdot)$, as seen in Figure 3 for the rotational dynamics. In this structure, we subtract τ_β from the saturation limits, and then, the output of the saturation function is added to τ_β. Note that the two structures illustrated in Figure 3 are equivalent. A similar saturation function with modified limits is proposed for the translational dynamics, as seen in Figure 4. In the following subsections, we make use of these proposed structures in the design of the AWC-based attitude and velocity controllers.

3.1.1 AWC-based attitude controller

Theorem 3.1: *Consider the rotational dynamics (6), Assumption 2.2, and the AWC-based attitude controller (11). If there exist a positive definite matrix $K_\omega \in \mathbb{R}^{3\times3}$ and positive diagonal matrices $Y, V \in \mathbb{R}^{3\times3}$ such that the following LMI is feasible:*

$$\begin{bmatrix} -\frac{1}{2}(K_\omega + K'_\omega) & -\frac{1}{2}(Y + V + K'_\omega) \\ * & -(Y+V) \end{bmatrix} \leq 0, \tag{20}$$

then with $K_a = YV^{-1}$, it can be concluded that $\omega \to \omega_d$.

Proof of Theorem: For the sake of brevity, we define $\underline{\tau}_n := \underline{\tau} - \tau_\beta$ and $\overline{\tau}_n := \overline{\tau} - \tau_\beta$. Utilizing the proposed saturation function in Figure 3, the rotational dynamics (6) can be rewritten as:

$$J\dot{\omega} = -\omega \times J\omega + \tau_\beta + \text{sat}_{\underline{\tau}_n}^{\overline{\tau}_n}(\tau_C + \tau_A). \tag{21}$$

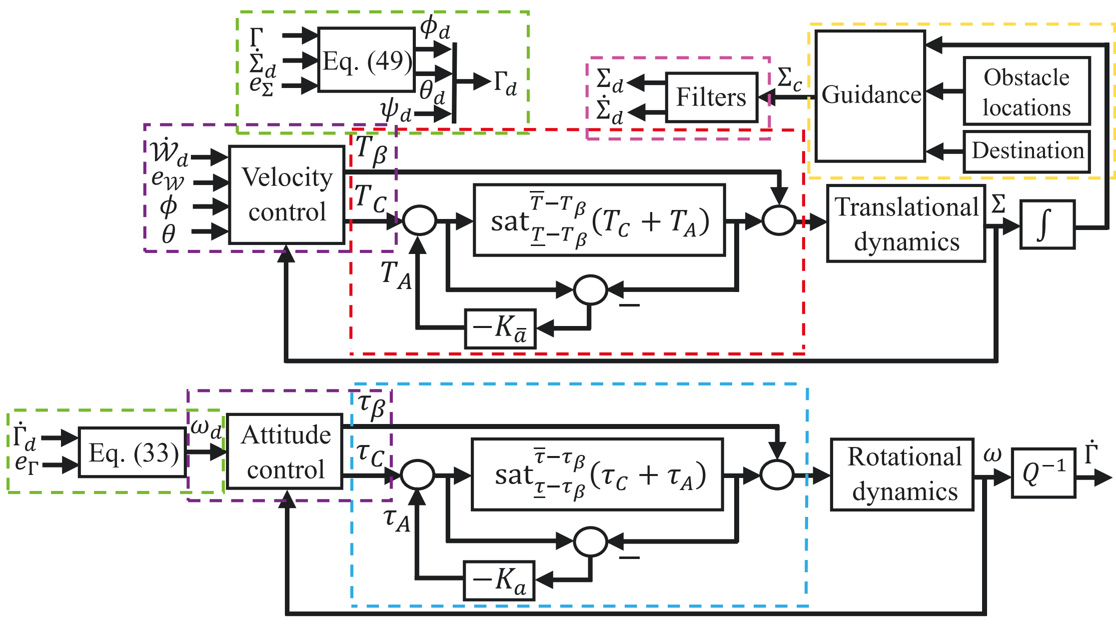

Figure 2. Full schematic of the proposed integrated control and guidance approach.

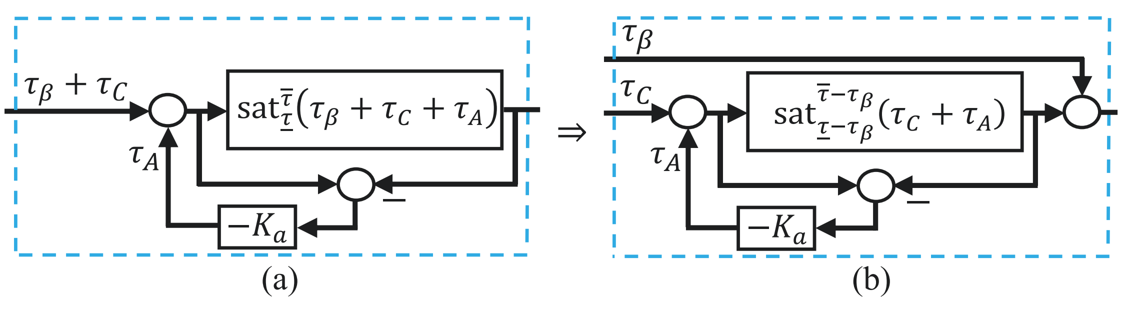

Figure 3. AWC-based control structure for rotational dynamics: a) saturation function with actual limits b) proposed saturation function with modified limits.

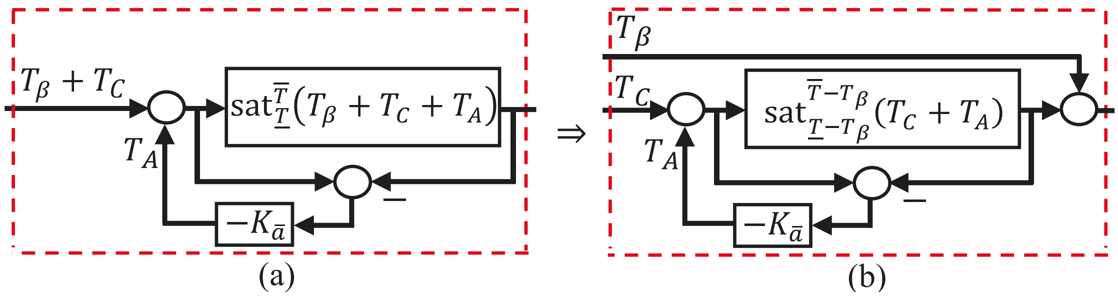

Figure 4. AWC-based control structure for translational dynamics: a) saturation function with actual limits b) proposed saturation function with modified limits.

Substituting (2) into (21) yields

$$J\dot{\omega} = -\omega \times J\omega + \tau - \mathrm{Dz}_{\underline{\tau}_n}^{\overline{\tau}_n}(\tau_C + \tau_A). \tag{22}$$

Inserting the control torque (11) into (22) leads to

$$J\dot{e}_\omega = -e_\omega \times J\omega - K_\omega e_\omega - (K_a + \mathcal{I})\mathrm{Dz}_{\underline{\tau}_n}^{\overline{\tau}_n}(\tau_C + \tau_A), \tag{23}$$

where $\mathcal{I}$ is an identity matrix.

Now, let us consider the following Lyapunov function candidate:

$$V(e_\omega) = \frac{1}{2}e_\omega' J e_\omega. \tag{24}$$

Calculating the time-derivative of $V(e_\omega)$ along the solutions of (23) leads to

$$\begin{aligned}\dot{V}(e_\omega) = e_\omega'[&-e_\omega \times J\omega - (K_\omega + K_\omega')e_\omega \\ &- (K_a + \mathcal{I})\mathrm{Dz}_{\underline{\tau}_n}^{\overline{\tau}_n}(\tau_C + \tau_A)].\end{aligned} \tag{25}$$

Noting that $e_\omega'(-e_\omega \times J\omega) = 0$, the above equation can be simplified to

$$\dot{V}(e_\omega) = -e_\omega'(K_\omega + K_\omega')e_\omega - e_\omega'(K_a + \mathcal{I})\mathrm{Dz}_{\underline{\tau}_n}^{\overline{\tau}_n}(\tau_C + \tau_A). \tag{26}$$

If $\mathrm{Dz}_{\underline{\tau}_n}^{\overline{\tau}_n}(\tau_C + \tau_A) = 0$, the control torques do not exceed the saturation bounds. Therefore, in this case, it is evident from (26) that the following condition should be satisfied for the asymptotic stability of the rotational dynamics:

$$K_\omega + K_\omega' > 0. \tag{27}$$

According to the proof of Lemma 2.1 and Assumption 2.2, if saturation occurs (i.e. $\mathrm{Dz}_{\underline{\tau}_n}^{\overline{\tau}_n}(\tau_C + \tau_A) \neq 0$), the following sector condition is satisfied for a positive diagonal matrix $\mathscr{W} \in \mathbb{R}^{3\times 3}$:

$$\mathrm{sat}_{\underline{\tau}_n}^{\overline{\tau}_n}(\tau_C + \tau_A)'\mathscr{W}\mathrm{Dz}_{\underline{\tau}_n}^{\overline{\tau}_n}(\tau_C + \tau_A) > 0. \tag{28}$$

The above inequality can be rewritten as

$$[\tau_C + \tau_A - \mathrm{Dz}_{\underline{\tau}_n}^{\overline{\tau}_n}(\tau_C + \tau_A)]'\mathscr{W}\mathrm{Dz}_{\underline{\tau}_n}^{\overline{\tau}_n}(\tau_C + \tau_A) > 0. \tag{29}$$

According to (11), condition (29) can be rewritten as

$$[-K_\omega e_\omega - (K_a + \mathcal{I})\mathrm{Dz}_{\underline{\tau}_n}^{\overline{\tau}_n}(\tau_C + \tau_A)]'\mathscr{W}\mathrm{Dz}_{\underline{\tau}_n}^{\overline{\tau}_n}(\tau_C + \tau_A) > 0. \tag{30}$$

By combining (26) and (30), we can deduce that $\dot{V}(e_\omega) < 0$ if

$$\eta' \underbrace{\begin{bmatrix} -\frac{1}{2}(K_\omega + K_\omega') & -\frac{1}{2}(K_a + \mathcal{I} + K_\omega'\mathscr{W}) \\ * & -(K_a + \mathcal{I})\mathscr{W} \end{bmatrix}}_{\Upsilon} \eta \le 0, \tag{31}$$

where $\eta = [e_\omega \quad \mathrm{Dz}_{\underline{\tau}_n}^{\overline{\tau}_n}(\tau_C + \tau_A)]'$. Pre- and post-multiplying both sides of $\Upsilon \le 0$ by $\mathrm{diag}\{\mathcal{I}, \mathscr{W}^{-1}\}$ yields

$$\begin{bmatrix} -\frac{1}{2}(K_\omega + K_\omega') & -\frac{1}{2}(K_a\mathscr{W}^{-1} + \mathscr{W}^{-1} + K_\omega{}') \\ * & -(\mathscr{W}^{-1}K_a + \mathscr{W}^{-1}) \end{bmatrix} \le 0. \tag{32}$$

Notice that K_a and $\mathscr{W}$ are diagonal matrices, therefore $K_a\mathscr{W}^{-1} = \mathscr{W}^{-1}K_a$. Letting $V = \mathscr{W}^{-1}$ and $Y = K_a\mathscr{W}^{-1}$ in (32) leads to the condition (20). ■

Proposition 3.1: *If under the conditions of Theorem 3.1, the AWC-based attitude controller (11) is designed, and the desired angular velocity is calculated as*

$$\omega_d = Q(\dot{\Gamma}_d - K_\Gamma e_\Gamma), \tag{33}$$

where K_Γ is a positive matrix, $e_\Gamma := \Gamma - \Gamma_d$, and $\Gamma_d = [\phi_d, \theta_d, \psi_d]'$, it can be concluded that $\Gamma \to \Gamma_d$.

Proof of Proposition: Subtracting (8) and (33) leads to

$$e_\omega = Q(\dot{\Gamma} - \dot{\Gamma}_d + K_\Gamma e_\Gamma) = Q(\dot{e}_\Gamma + K_\Gamma e_\Gamma). \tag{34}$$

Since $e_\omega \to 0$, it follows from (34) that

$$\dot{e}_\Gamma + K_\Gamma e_\Gamma \to 0. \tag{35}$$

We can conclude from (35) that $e_\Gamma \to 0$, which implies $\Gamma \to \Gamma_d$. ■

3.1.2 AWC-based velocity control

First, we present some definitions that are used in the following. Let $\Sigma := [\mathcal{U}, \mathcal{V}, \mathcal{W}]'$ be the translational velocities in the x-, y-, and z-directions, respectively, and $\Sigma_d := [\mathcal{U}_d, \mathcal{V}_d, \mathcal{W}_d]'$ are the corresponding desired translational velocities. The translational velocity errors are defined as $e_\Sigma := [e_\mathcal{U}, e_\mathcal{V}, e_\mathcal{W}]'$, where $e_\mathcal{U} := \mathcal{U} - \mathcal{U}_d$, $e_\mathcal{V} := \mathcal{V} - \mathcal{V}_d$, and $e_\mathcal{W} := \mathcal{W} - \mathcal{W}_d$.

Theorem 3.2: *Consider the third equation in the translational dynamics* (5), *Assumption 2.3, and the AWC-based velocity controller* (12). *If there exist positive scalars $K_\mathcal{W}, \hat{Y}, \hat{V}$ such that the following LMI is feasible:*

$$\begin{bmatrix} -K_\mathcal{W} & \frac{1}{2}[(\hat{V}+\hat{Y})/m + mK_\mathcal{W}] \\ * & -(\hat{V}+\hat{Y}) \end{bmatrix} \leq 0, \tag{36}$$

where $K_{\bar{a}} = \hat{Y}\hat{V}^{-1}$, it can be concluded that $\mathcal{W} \to \mathcal{W}_d$.

Proof of Theorem: Utilizing the proposed saturation function in Figure 4, the third equation in (5) can be rewritten as:

$$\ddot{z} = g - \frac{T_\beta}{m}c_\phi c_\theta - \frac{\mathrm{sat}_{\underline{T}_n}^{\overline{T}_n}(T_C + T_A)}{m}c_\phi c_\theta, \tag{37}$$

where $\underline{T}_n := \underline{T} - T_\beta$ and $\overline{T}_n := \overline{T} - T_\beta$. Substituting (2) into (37) results in

$$\ddot{z} = g - \frac{T}{m}c_\phi c_\theta + \frac{\mathrm{Dz}_{\underline{T}_n}^{\overline{T}_n}(T_C + T_A)}{m}c_\phi c_\theta. \tag{38}$$

Inserting the control thrust (12) into (38) results in

$$\dot{e}_\mathcal{W} = -K_\mathcal{W}e_\mathcal{W} + \left(\frac{1+K_{\bar{a}}}{m}\right)c_\phi c_\theta \mathrm{Dz}_{\underline{T}_n}^{\overline{T}_n}(T_C + T_A). \tag{39}$$

We now consider the Lyapunov function candidate as:

$$V(e_\mathcal{W}) = \frac{1}{2}{e_\mathcal{W}}^2. \tag{40}$$

Taking the derivative of $V(e_\mathcal{W})$ along the solutions of (38) yields

$$\dot{V}(e_\mathcal{W}) = e_\mathcal{W}\left[-K_\mathcal{W}e_\mathcal{W} + \left(\frac{1+K_{\bar{a}}}{m}\right)c_\phi c_\theta \mathrm{Dz}_{\underline{T}_n}^{\overline{T}_n}(T_C + T_A)\right]. \tag{41}$$

The expression $\mathrm{Dz}_{\underline{T}_n}^{\overline{T}_n}(T_C + T_A) = 0$ means that the control thrust lies within the saturation limits. Therefore, in this case, it is enough for ensuring asymptotic stability that $K_\mathcal{W}$ be a positive scalar.

Based on the proof of Lemma 2.1 and Assumption 2.3, if saturation occurs (i.e. $\mathrm{Dz}_{\underline{T}_n}^{\overline{T}_n}(T_C + T_A) \neq 0$), the following sector condition holds for a positive scalar $\hat{\mathscr{W}}$:

$$\mathrm{sat}_{\underline{T}_n}^{\overline{T}_n}(T_C + T_A)\hat{\mathscr{W}}\mathrm{Dz}_{\underline{T}_n}^{\overline{T}_n}(T_C + T_A) > 0, \tag{42}$$

which is equivalent to

$$[T_C + T_A - \mathrm{Dz}_{\underline{T}_n}^{\overline{T}_n}(T_C + T_A)]\hat{\mathscr{W}}\mathrm{Dz}_{\underline{T}_n}^{\overline{T}_n}(T_C + T_A) > 0. \tag{43}$$

According to (12), the condition (43) can be rewritten as

$$\left[\frac{m}{c_\phi c_\theta}K_\mathcal{W}e_\mathcal{W} - (1+K_{\bar{a}})\,\mathrm{Dz}_{\underline{T}_n}^{\overline{T}_n}(T_C + T_A)\right] \times \hat{\mathscr{W}}\mathrm{Dz}_{\underline{T}_n}^{\overline{T}_n}(T_C + T_A) > 0. \tag{44}$$

According to Assumption 2.1, since $\phi, \theta \neq \pm\pi/2$, then $(c_\phi c_\theta)^2 > 0\ \forall t$. Therefore, (44) can be multiplied by $(c_\phi c_\theta)^2$:

$$[mK_\mathcal{W}e_\mathcal{W} - (1+K_{\bar{a}})c_\phi c_\theta\,\mathrm{Dz}_{\underline{T}_n}^{\overline{T}_n}(T_C + T_A)] \times \hat{\mathscr{W}}c_\phi c_\theta\mathrm{Dz}_{\underline{T}_n}^{\overline{T}_n}(T_C + T_A) > 0. \tag{45}$$

After adding the left-hand side of (45) to (41), we can conclude that $\dot{V}(e_\mathcal{W}) < 0$ if

$$\xi'\underbrace{\begin{bmatrix} -K_\mathcal{W} & \frac{1}{2}[(1+K_{\bar{a}})/m + mK_\mathcal{W}\hat{\mathscr{W}}] \\ * & -(1+K_{\bar{a}})\hat{\mathscr{W}} \end{bmatrix}}_{\Pi}\xi \leq 0, \tag{46}$$

where $\xi = [e_\mathcal{W}\ \ \mathrm{Dz}_{\underline{T}_n}^{\overline{T}_n}(T_C + T_A)c_\phi c_\theta]'$. Pre- and post-multiplying both sides of $\Pi \leq 0$ by diag$\{1, \hat{\mathscr{W}}^{-1}\}$ results in

$$\begin{bmatrix} -K_\mathcal{W} & \frac{1}{2}[(\hat{\mathscr{W}}^{-1} + K_{\bar{a}}\hat{\mathscr{W}}^{-1})/m + mK_\mathcal{W}] \\ * & -(\hat{\mathscr{W}}^{-1} + \hat{\mathscr{W}}^{-1}K_{\bar{a}}) \end{bmatrix} \leq 0. \tag{47}$$

Notice that $K_{\bar{a}}$ and $\hat{\mathscr{W}}$ are positive scalars, therefore $K_{\bar{a}}\hat{\mathscr{W}}^{-1} = \hat{\mathscr{W}}^{-1}K_{\bar{a}}$. By letting $\hat{V} = \hat{\mathscr{W}}^{-1}$ and $\hat{Y} = K_{\bar{a}}\hat{\mathscr{W}}^{-1}$ in (47), condition (36) is obtained. ■

Remark 3.1: Determining the desired roll and pitch angles is nontrivial since the x and y positions are controlled via the roll and pitch of the vehicle. Therefore, the roll and pitch angles can be obtained from the translational dynamics (Elkholy & Habib, 2019),

$$\begin{aligned} \theta &= \tan^{-1}\left[\frac{\dot{\mathcal{U}}c_\psi + \dot{\mathcal{V}}s_\psi}{\dot{\mathcal{W}}_d - K_\mathcal{W}e_\mathcal{W} - g}\right], \\ \phi &= \tan^{-1}\left[\frac{\dot{\mathcal{U}}c_\theta s_\psi - \dot{\mathcal{V}}c_\theta c_\psi}{\dot{\mathcal{W}}_d - K_\mathcal{W}e_\mathcal{W} - g}\right]. \end{aligned} \tag{48}$$

We therefore define the desired roll and pitch angles as

$$\begin{aligned} \theta_d &= \tan^{-1}\left[\frac{(\dot{\mathcal{U}}_d - K_\mathcal{U}e_\mathcal{U})\,c_\psi + (\dot{\mathcal{V}}_d - K_\mathcal{V}e_\mathcal{V})\,s_\psi}{\dot{\mathcal{W}}_d - K_\mathcal{W}e_\mathcal{W} - g}\right], \\ \phi_d &= \tan^{-1}\left[\frac{(\dot{\mathcal{U}}_d - K_\mathcal{U}e_\mathcal{U})\,c_\theta s_\psi - (\dot{\mathcal{V}}_d - K_\mathcal{V}e_\mathcal{V})\,c_\theta c_\psi}{\dot{\mathcal{W}}_d - K_\mathcal{W}e_\mathcal{W} - g}\right], \end{aligned} \tag{49}$$

where $K_{\mathcal{U}}$ and $K_{\mathcal{V}}$ are the positive velocity gains. From Proposition 3.1, we have that $\Gamma \to \Gamma_d$, which implies that $\phi \to \phi_d$ and $\theta \to \theta_d$. Therefore, from (48) and (49), we can conclude that

$$\begin{aligned} \dot{\mathcal{U}} &\to \dot{\mathcal{U}}_d - K_{\mathcal{U}} e_{\mathcal{U}}, \\ \dot{\mathcal{V}} &\to \dot{\mathcal{V}}_d - K_{\mathcal{V}} e_{\mathcal{V}}. \end{aligned} \tag{50}$$

It follows from (50) that

$$\begin{aligned} \dot{e}_{\mathcal{U}} + K_{\mathcal{U}} e_{\mathcal{U}} &\to 0, \\ \dot{e}_{\mathcal{V}} + K_{\mathcal{V}} e_{\mathcal{V}} &\to 0, \end{aligned} \tag{51}$$

which imply that $e_{\mathcal{U}} \to 0$ and $e_{\mathcal{V}} \to 0$.

Remark 3.2: The desired yaw angle ψ_d is typically set to zero and is only nonzero if the quadrotor requires rotation for pointing the object detection sensor. In this study, we assume that obstacles can be detected without the need to rotate the vehicle, therefore, $\psi_d = 0$.

Remark 3.3: The proposed structures illustrated in Figures 3 and 4 are utilised to obtain the LMI conditions (20) and (36). More precisely, the key role of the proposed structures can be seen in sector conditions (28) and (42) where the signals τ_β and T_β are absent. Otherwise, if a standard sector where used, τ_β and T_β would appear in these sector conditions, leading to a less tractable design solution.

3.2 Guidance

For autonomous guidance and navigation, a quadrotor must possess the capability to move from one position to another while avoiding obstacles. In this subsubsection, an algorithm, which is borrowed from Kirven and Hoagg (2021), is described for generating the desired translational velocities to achieve collision avoidance and destination-seeking goals.

The guidance method includes two components:

- Obstacle avoidance (repulsive) component,
- The destination seeking (attractive) component.

These two components make up $\Sigma_c = [\mathcal{U}_c,\ \mathcal{V}_c, \mathcal{W}_c]'$, indicating the velocity commands in the x-, y-, and z-directions, respectively

$$\begin{bmatrix} \mathcal{U}_c \\ \mathcal{V}_c \\ \mathcal{W}_c \end{bmatrix} = \begin{bmatrix} \mathcal{U}_{\text{rep}} \\ \mathcal{V}_{\text{rep}} \\ \mathcal{W}_{\text{rep}} \end{bmatrix} + \begin{bmatrix} \mathcal{U}_{\text{attr}} \\ \mathcal{V}_{\text{attr}} \\ \mathcal{W}_{\text{attr}} \end{bmatrix}. \tag{52}$$

We now present the repulsive and attractive components.

- Obstacle avoidance (repulsive component):
  Let $p_j := [p_{1_j}, p_{2_j}, p_{3_j}]'$ be the position of the jth point on an obstacle relative to o_B, resolved in B for $j \in \{1, \dots, n\}$. To generate the obstacle avoidance component of the velocity commands, consider the following ellipsoids:

$$E_i := \left\{ p_j \in \mathbb{R}^3 : \frac{p_{1_j}^{\,2}}{a_i^2} + \frac{p_{2_j}^{\,2}}{b_i^2} + \frac{p_{3_j}^{\,2}}{c_i^2} \le 1 \right\},$$

$$E_o := \left\{ p_j \in \mathbb{R}^3 : \frac{p_{1_j}^{\,2}}{a_o^2} + \frac{p_{2_j}^{\,2}}{b_o^2} + \frac{p_{3_j}^{\,2}}{c_o^2} \le 1 \right\}. \tag{53}$$

where E_i and E_o are, respectively, the inner and outer ellipsoids of a potential field. If $p_j \in E_i$ (E_o), it means that p_j lies inside a physical ellipsoid with a geometric centre at o_B and semi-principal axes $a_i\hat{b}_1, b_i\hat{b}_2$, and $c_i\hat{b}_3$ ($a_o\hat{b}_1, b_o\hat{b}_2$, and $c_o\hat{b}_3$). Consider the following the potential field:

$$U(p_j) = \begin{cases} 0, & \text{if } p_j \in \mathbb{R}^3 \backslash E_o, \\ U_{\max} \left(\frac{r_o(p_j) - \|p_j\|}{r_o(p_j) - r_i(p_j)} \right), & \text{if } p_j \in E_o \backslash E_i, \\ U_{\max}, & \text{if } p_j \in E_i, \end{cases} \tag{54}$$

where $U_{\max} > 0$ is the maximum potential,

$$\begin{aligned} r_i(p_j) &:= \left[\left(a_i^2 \cos^2 \beta_i(p_j) + b_i^2 \sin^2 \beta_i(p_j) \right) \cos^2 \alpha_i(p_j) \right. \\ &\quad \left. + c_i^2 \sin^2 \alpha_i(p_j) \right]^{1/2}, \\ r_o(p_j) &:= \left[\left(a_o^2 \cos^2 \beta_o(p_j) + b_o^2 \sin^2 \beta_o(p_j) \right) \cos^2 \alpha_o(p_j) \right. \\ &\quad \left. + c_o^2 \sin^2 \alpha_o(p_j) \right]^{1/2}, \end{aligned}$$

and

$$\alpha_i(p_j) := \tan^{-1} \left(\frac{p_{3j}/c_i}{\sqrt{{p_{1j}}^2/a_i^2 + {p_{2j}}^2/b_i^2}} \right),$$

$$\alpha_o(p_j) := \tan^{-1} \left(\frac{p_{3j}/c_o}{\sqrt{{p_{1j}}^2/a_o^2 + {p_{2j}}^2/b_o^2}} \right),$$

$$\beta_i(p_j) := \text{arctan}\,2 \left(p_{2j}/b_i, p_{1j}/a_i \right),$$

$$\beta_o(p_j) := \text{arctan}\,2 \left(p_{2j}/b_o, p_{1j}/a_o \right).$$

Now, the repulsive component is considered as

$$\begin{bmatrix} \mathcal{U}_{\text{rep}} \\ \mathcal{V}_{\text{rep}} \\ \mathcal{W}_{\text{rep}} \end{bmatrix} = -\frac{1}{n_e} \sum_{j=1}^{n} U\left(p_j\right) \frac{\mathcal{O}' p_j}{\|p_j\|}, \tag{55}$$

where n_e is the number of obstacle points contained in E_o.

- Destination seeking (attractive component):

The destination seeking component of the velocity commands is defined as:

$$\begin{bmatrix} \mathcal{U}_{\text{attr}} \\ \mathcal{V}_{\text{attr}} \\ \mathcal{W}_{\text{attr}} \end{bmatrix} = \begin{cases} \frac{s_d p_g}{\|p_g\|}, & \text{if } \|p_g\| \ge d_s, \\ \frac{s_d p_g}{d_s}, & \text{if } \|p_g\| < d_s, \end{cases} \tag{56}$$

where p_g is the position of the destination relative to o_B, resolved in I, s_d is the desired speed, and d_s is the stopping distance.

After obtaining the repulsive and attractive components, the velocity commands Σ_c from (52) are passed through a fourth-order low-pass filter with unity gain at DC, which produces the desired translational velocities $\mathcal{U}_d, \mathcal{V}_d$, and $\mathcal{W}_d$ and their derivatives. Specifically, consider the following filter transfer function:

$$\frac{\mathcal{U}_d(s)}{\mathcal{U}_c(s)} = \frac{\alpha_0}{s^4 + \alpha_3 s^3 + \alpha_2 s^2 + \alpha_1 s + \alpha_0}. \tag{57}$$

Therefore, $\mathcal{U}_d(t)$ satisfies

$$\begin{bmatrix} \ddddot{\mathcal{U}}_d \\ \dddot{\mathcal{U}}_d \\ \ddot{\mathcal{U}}_d \\ \dot{\mathcal{U}}_d \end{bmatrix} = \begin{bmatrix} -\alpha_3 & -\alpha_2 & -\alpha_1 & -\alpha_0 \\ 1 & 0 & 0 & 0 \\ 0 & 1 & 0 & 0 \\ 0 & 0 & 1 & 0 \end{bmatrix} \begin{bmatrix} \dddot{\mathcal{U}}_d \\ \ddot{\mathcal{U}}_d \\ \dot{\mathcal{U}}_d \\ \mathcal{U}_d \end{bmatrix} + \begin{bmatrix} \alpha_0 \\ 0 \\ 0 \\ 0 \end{bmatrix} \mathcal{U}_c, \tag{58}$$

which can be solved to obtain $\mathcal{U}_d$ and $\dot{\mathcal{U}}_d$. In the same way, one can obtain $\mathcal{V}_d, \mathcal{W}_d$ and their derivatives.

Remark 3.4: As can be seen from (56), the goal speed is proportional to its distance to the destination if the quadrotor is closer than d_s to the destination. On the other hand, the goal speed is constant if the quadrotor is farther than d_s from the destination.

4. Simulation results

In this section, the following three cases are simulated to illustrate the performance of our method:

- Case 1: Without saturation
- Case 2: With saturation – Without AWC
- Case 3: With saturation – With AWC

For the simulation, we consider the following parameters:

$$m = 1.01\,\text{kg}, \quad l = 0.1185\,\text{m}, \quad k = 7.5 \times 10^{-6}\,\text{kg} \cdot \text{m/rad}^2,$$
$$b = 1.4 \times 10^{-7}\,\text{kg} \cdot \text{m}^2/\text{rad}^2, \quad \overline{\varpi} = 630\,\text{rad/s}, \quad K_\Gamma = 4\mathcal{I}$$
$$J = \text{diag}(0.00585, 0.0054, 0.007), \quad K_{\mathcal{U}} = 2, \quad K_{\mathcal{V}} = 2.$$

Let the guidance parameters be

$$a_i = 0.85\,\text{m}, \quad b_i = 0.7\,\text{m}, \quad c_i = 0.35\,\text{m},$$
$$a_o = 1.65\,\text{m}, \quad b_o = 1.15\,\text{m}, \quad c_o = 0.85\,\text{m},$$
$$s_d = 2.9\,\text{m /s}, \quad d_s = 2.9\,\text{m}, \quad U_{\max} = 5.8\,\text{m/s}.$$

All the poles of the low-pass filter transfer function are placed at -10. The starting and the destination coordinates are $[-0.2, 2, 3]'$ and $[4, 0, 1.1]'$, respectively. The desired yaw ψ_d is set to zero. Also, to induce saturation of the propellers, a simplified wind disturbance is considered: a rectangular signal with a magnitude equivalent to 67.19% of the maximum thrust generated by a single propeller (i.e. $0.6719\,k\overline{\varpi}^2$) is applied in the positive y-direction over the time interval of 1s to 3s.

By using the YALMIP toolbox (Lofberg, 2004) and MOSEK solver (ApS, 2023), the LMIs (20) and (36) are solved to calculate the controller and AWC gains:

$$K_\omega = 0.8915\mathcal{I}, \quad K_{\mathcal{W}} = 0.9019, \quad K_a = \mathcal{I}, \quad K_{\bar{a}} = 1.$$

Remark 4.1: As can be seen from Figures 3 and 4, the two structures are equivalent to each other, where

$$\text{sat}_{\underline{\tau}}^{\overline{\tau}}(\tau_\beta + \tau_C + \tau_A) = \tau_\beta + \text{sat}_{\underline{\tau}-\tau_\beta}^{\overline{\tau}-\tau_\beta}(\tau_C + \tau_A), \tag{59}$$

$$\text{sat}_{\underline{T}}^{\overline{T}}(T_\beta + T_C + T_A) = T_\beta + \text{sat}_{\underline{T}-T_\beta}^{\overline{T}-T_\beta}(T_C + T_A), \tag{60}$$

and

$$\text{Dz}_{\underline{\tau}}^{\overline{\tau}}(\tau_\beta + \tau_C + \tau_A) = \text{Dz}_{\underline{\tau}-\tau_\beta}^{\overline{\tau}-\tau_\beta}(\tau_C + \tau_A), \tag{61}$$

$$\text{Dz}_{\underline{T}}^{\overline{T}}(T_\beta + T_C + T_A) = \text{Dz}_{\underline{T}-T_\beta}^{\overline{T}-T_\beta}(T_C + T_A). \tag{62}$$

Therefore, for simulation, the left-hand side of the deadzones (61) and (62) are used in place of the terms τ_A and T_A, respectively, in the AWC-based controllers (11) and (12).

Remark 4.2: For quadrotors, the mechanism that causes saturation is propeller speed, which occurs when the motors driving the propellers reach their maximum rotational speed and cannot increase their speed any further to generate additional thrust or torque. However, as seen from Figures 3 and 4, the controller produces torque and thrust commands while the UAV (and AWC) are driven by the saturation (and deadzone) of the torques and thrust. Therefore, we obtain $\text{sat}_{\underline{T}}^{\overline{T}}(T)$ and $\text{sat}_{\underline{\tau}_i}^{\overline{\tau}_i}(\tau_i)$ by perform the following real-time operations in simulation:

$$\begin{bmatrix} \varpi_1^2 \\ \varpi_2^2 \\ \varpi_3^2 \\ \varpi_4^2 \end{bmatrix} = \underbrace{\begin{bmatrix} \frac{1}{4k} & \frac{1}{4kl} & \frac{1}{4kl} & \frac{1}{4b} \\ \frac{1}{4k} & \frac{-1}{4kl} & \frac{1}{4kl} & \frac{-1}{4b} \\ \frac{1}{4k} & \frac{-1}{4kl} & \frac{-1}{4kl} & \frac{1}{4b} \\ \frac{1}{4k} & \frac{1}{4kl} & \frac{-1}{4kl} & \frac{-1}{4b} \end{bmatrix}}_{\mathcal{S}} \begin{bmatrix} T \\ \tau_1 \\ \tau_2 \\ \tau_3 \end{bmatrix}. \tag{63}$$

With propeller speed limited by $\text{sat}_0^{\overline{\varpi}^2}(\varpi_i^2),\ i = \{1, \ldots, 4\}$, one can obtain:

$$\begin{bmatrix} \text{sat}_{\underline{T}}^{\overline{T}}(T) \\ \text{sat}_{\underline{\tau}_1}^{\overline{\tau}_1}(\tau_1) \\ \text{sat}_{\underline{\tau}_2}^{\overline{\tau}_2}(\tau_2) \\ \text{sat}_{\underline{\tau}_3}^{\overline{\tau}_3}(\tau_3) \end{bmatrix} = \underbrace{\begin{bmatrix} k & k & k & k \\ kl & -kl & -kl & kl \\ kl & kl & -kl & -kl \\ b & -b & b & -b \end{bmatrix}}_{\mathcal{S}^{-1}} \begin{bmatrix} \text{sat}_0^{\overline{\varpi}^2}(\varpi_1^2) \\ \text{sat}_0^{\overline{\varpi}^2}(\varpi_2^2) \\ \text{sat}_0^{\overline{\varpi}^2}(\varpi_3^2) \\ \text{sat}_0^{\overline{\varpi}^2}(\varpi_4^2) \end{bmatrix}, \tag{64}$$

from which the deadzone functions of the control input thrust and torques can be calculated. The process of applying (63) and (64) in simulation of the quadrotor UAV is illustrated in Figure 5.

The quadrotor trajectories for the three cases are plotted in Figure 6. In Case 1, the saturation constraint is not applied in simulation. As expected, the green line shows that the quadrotor avoids all the obstacles and reaches the destination via a short route. However, it is evident from Figure 7 that the propeller speeds exceed the maximum propeller speed of $\overline{\varpi} = 630$ rad/s. In fact, the quadrotor has high maneuvering capabilities when propeller speed saturation is absent, allowing for a broader range of control inputs and enabling more flexible and efficient movement, particularly in navigating complex environments.

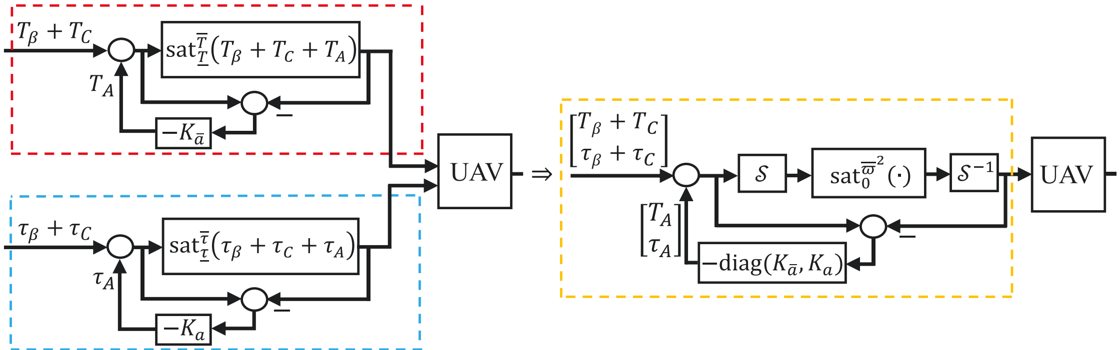

Figure 5. The process of applying the control strategy to the quadrotor UAV for simulation.

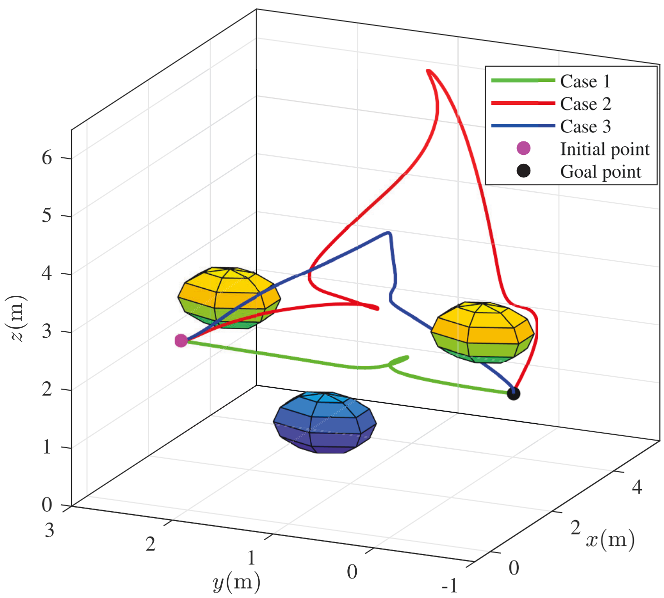

Figure 6. Comparison of the quadrotor trajectories.

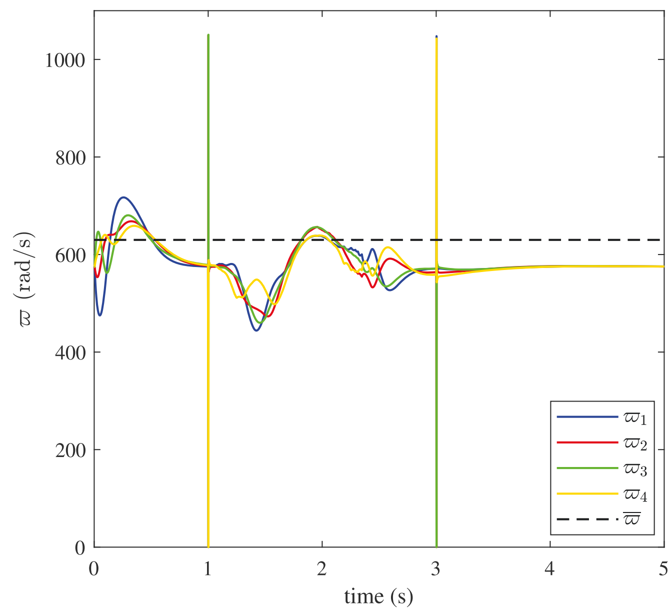

Figure 7. Propeller speed ϖ (Case 1).

In Case 2, the saturation constraint is applied in simulation but AWC is not implemented. The blue trajectory in Figure 6 illustrates that the quadrotor takes a significantly longer route to reach the destination. The observed deviation in the trajectory can be directly attributed to the saturation of propeller speeds, as depicted in Figure 8.

In Case 3, the saturation constraint is applied in simulation and AWC is implemented. Although saturation occurs (see Figure 9), the trajectory that the quadrotor follows to reach the destination is significantly shorter than the path of Case 2, as seen in Figure 6.

The distance from the quadrotor to the destination is presented in Figure 10. It is evident from this figure that, despite Case 3 not performing as well as Case 1, it is significantly better than Case 2. For a quantitative comparison, the distance travelled by the quadrotor in the three cases are provided in Table 1. This table indicates that the distance travelled in Case 3 is noticeably less than Case 2, but it is more than Case 1, which is the nominal case.

The translational velocities and Euler angles for Cases 1 and 3 are plotted in Figures 11–14. As can be observed from Figures 11 and 12, the system signals track the corresponding

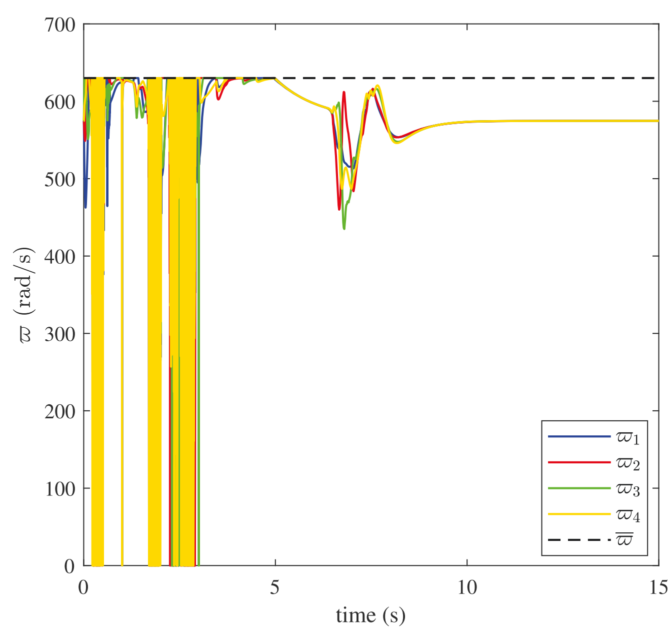

Figure 8. Propeller speed ϖ (Case 2).

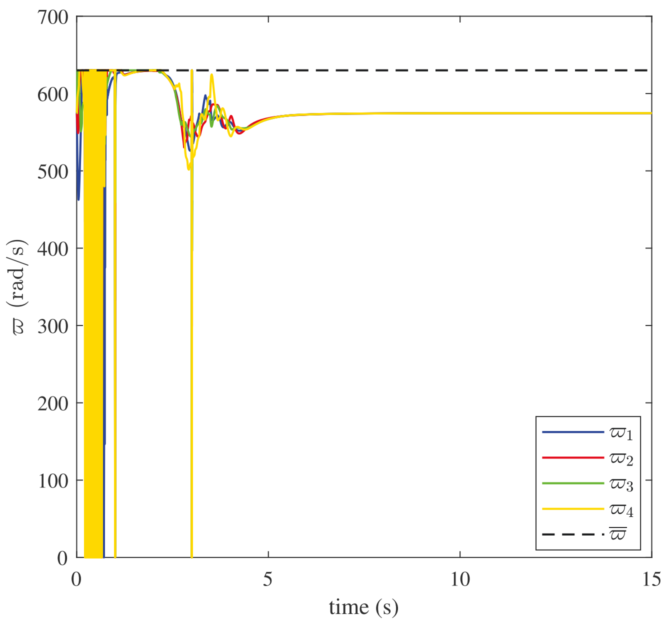

Figure 9. Propeller speed ϖ (Case 3).

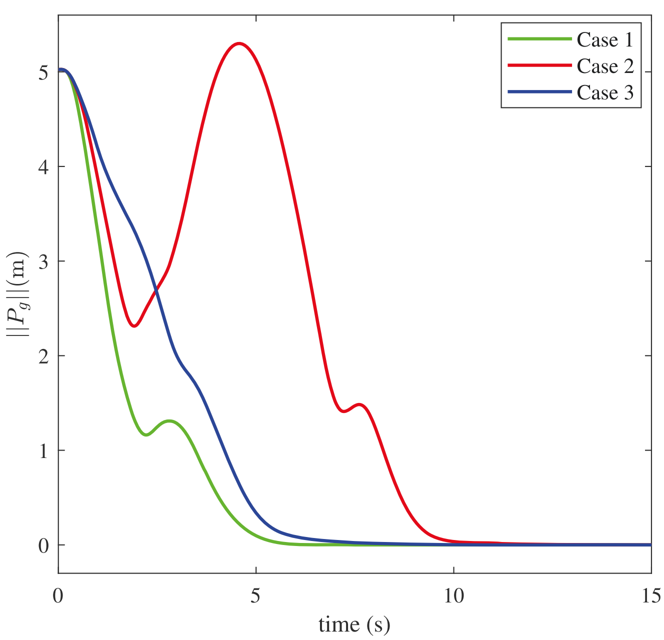

Figure 10. Distance from the quadrotor to the destination.

Table 1. Distance travelled by quadrotor.

Case 1	Case 2	Case 3
6.5729 (m)	14.9379 (m)	7.9182 (m)

desired signals accurately. It should be noted that the difference seen in tracking the desired signal in the middle subplot of Figure 12 is because of the disturbance in y-direction. On the other hand, we can see form Figures 13 and 14 that although there is deviation in the tracking of the desired signals due to the saturation of the propeller speeds in some time intervals, the signals due eventually track the corresponding desired signals.

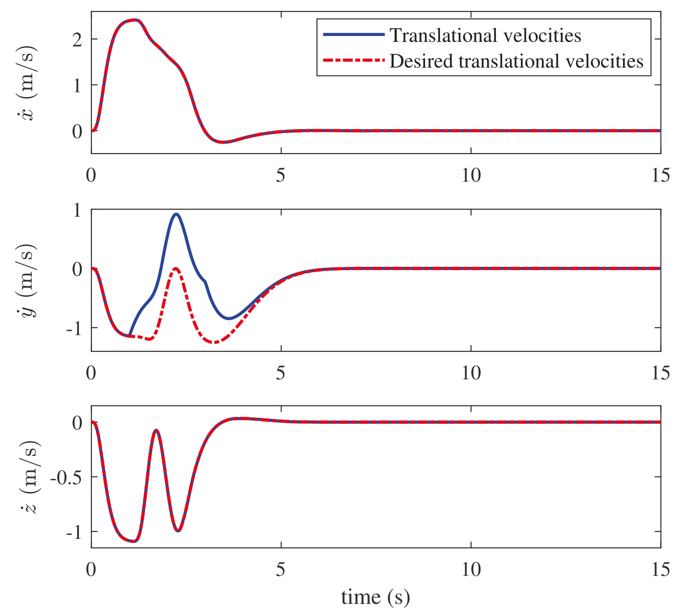

Figure 11. Translational velocities (Case 1).

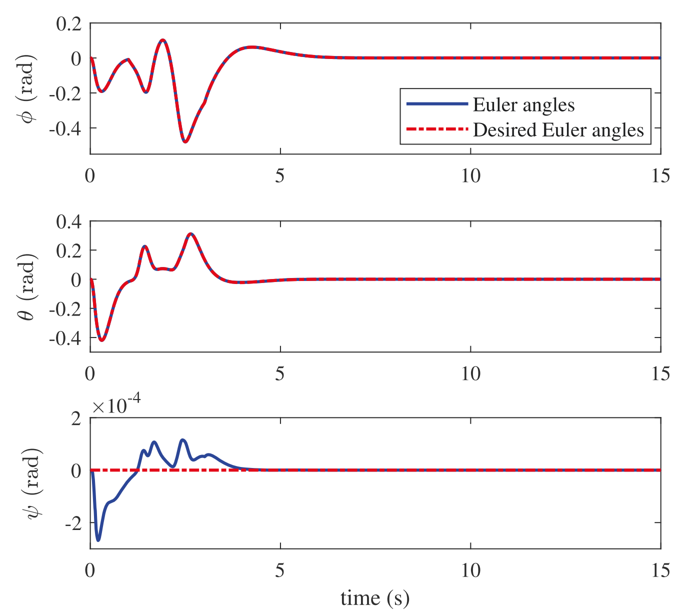

Figure 12. Euler angles (Case 1).

The simulation results illustrate an autonomous guidance mission when wind, which can be unavoidable during outdoor flight, is present. Case 2 illustrates how limited propeller speeds under this wind condition can lead to a longer path to the destination without the aid of AWC. Alternatively, Case 3 shows that this path can be significantly reduced with the use of the proposed static AWC. As a result, the static AWC leads to less power consumption, permitting the the vehicle to pursue further destinations than when AWC is absent.

5. Conclusion

In this paper, the constrained control problem is addressed for the autonomous guidance and control of quadrotors. This is motivated by missions where operating in windy conditions, the

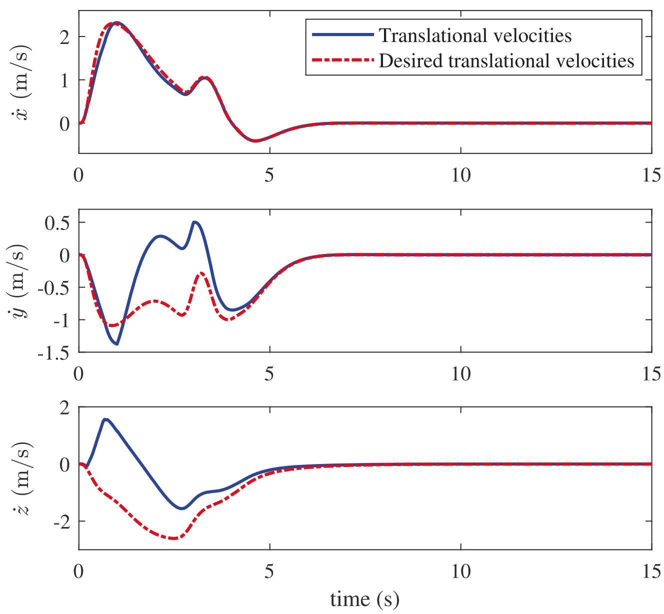

Figure 13. Translational velocities (Case 3).

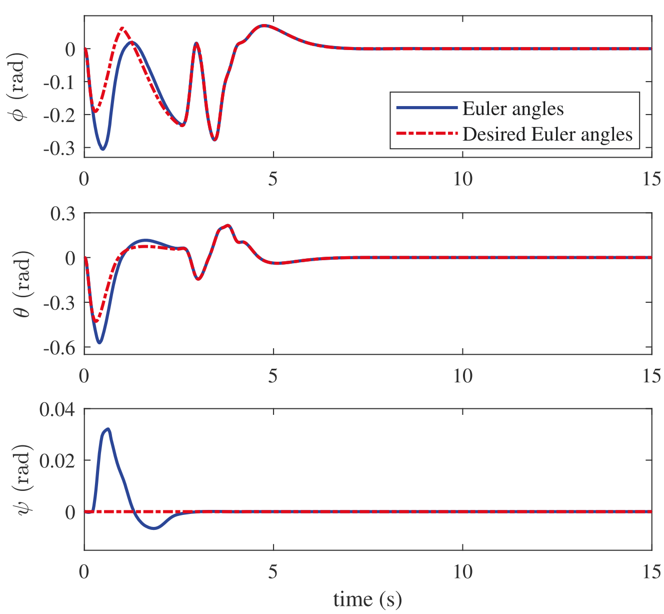

Figure 14. Euler angles (Case 3).

quadrotor's controller may demand excessive thrust to counteract wind, which can exceed the physical limits of the propellers and lead to actuator saturation. To address this issue, a static anti-windup compensator is designed to mitigate the effects of propeller speed saturation on the quadrotor's stability and control. Because of the coupled nonlinear dynamics that govern quadrotors, the challenge of designing an anti-windup compensator is solved via a novel reformulation of the saturation constraints. This new structure enables a linear matrix inequality formulation for determining the controller and anti-windup compensator gains. The effectiveness of the design method is illustrated through obstacle avoidance and destination seeking simulations of a quadrotor in an environment that contains wind and obstacles whose locations are unknown a priori but are measured in real-time.

This paper focuses on the saturation problem specifically related to limits on the magnitude of propeller speeds. Future research could explore the design of an anti-windup compensator that addresses not only the magnitude of propeller speeds but also rates at which the propellers change speed. This combined approach has the potential of significantly enhancing the performance of propeller systems across various applications. In addition, since dynamic anti-windup compensation is known to outperform static anti-windup compensation, future work will include the design of a dynamic anti-windup compensator for guidance and control of quadrotors.

Disclosure statement

No potential conflict of interest was reported by the author(s).

Funding

The material is based upon work supported by the National Science Foundation [award TI-2219008].

References

ApS, M. (2023). *The MOSEK optimization toolbox for MATLAB manual. Version 10.0.44* [Computer software manual].

Buratti, N., Invernizzi, D., & Lovera, M. (2019). Experimental validation of LMI-based anti-windup compensators for attitude control in multirotor UAVs. *IFAC-PapersOnLine*, *52*(12), 164–169. https://doi.org/10.1016/j.ifacol.2019.11.191

Chang, Z., Chu, H., & Shao, Y. (2023). Quadrotor trajectory-tracking control with actuator saturation. *Electronics*, *12*(3), 484. https://doi.org/10.3390/electronics12030484

Elkholy, H., & Habib, M. K. (2019). Dynamic modeling and control techniques for a quadrotor. In *Unmanned aerial vehicles: Breakthroughs in research and practice* (pp. 20–66). IGI global.

Falkenberg, O., Witt, J., Pilz, U., Weltin, U., & Werner, H. (2012). Model identification and attitude control for quadrotor MAV's. In *International Conference on Intelligent Robotics and Applications* (pp. 460–471).

Farber, B. E., & Richards, C. M. (2024). Adaptive control and parameter-dependent anti-windup compensation for inertia-varying quadcopters. *International Journal of Control*, *97*(2), 235–248. https://doi.org/10.1080/00207179.2022.2138555

Galeani, S., Tarbouriech, S., Turner, M., & Zaccarian, L. (2009). A tutorial on modern anti-windup design. *European Journal of Control*, *15*(3-4), 418–440. https://doi.org/10.3166/ejc.15.418-440

Ghignoni, P., Buratti, N., Invernizzi, D., & Lovera, M. (2020). Anti-windup design for directionality compensation with application to quadrotor UAVs. *IEEE Control Systems Letters*, *5*(1), 331–336.

Huang, B., Zhai, M., Lu, B., & Li, Q. (2022). Gain-scheduled anti-windup PID control for LPV systems under actuator saturation and its application to aircraft. *Aerospace Systems*, *5*(3), 445–454. https://doi.org/10.1007/s42401-022-00143-z

Jeon, H., Song, J., Lee, H., & Eun, Y. (2020). Modeling quadrotor dynamics in a wind field. *IEEE/ASME Transactions on Mechatronics*, *26*(3), 1401–1411. https://doi.org/10.1109/TMECH.2020.3019831

Kirven, T., & Hoagg, J. B. (2021). Autonomous quadrotor collision avoidance and destination seeking in a GPS-denied environment. *Autonomous Robots*, *45*, 99–118. https://doi.org/10.1007/s10514-020-09949-2

Liu, X., Sun, Q., & Hou, X. (2014). New approach on robust and reliable decentralized H_∞ tracking control for fuzzy interconnected systems with time-varying delay. *International Scholarly Research Notices*, *2014*(1), 705609.

Lofberg, J. (2004). YALMIP: A toolbox for modeling and optimization in MATLAB. In *2004 IEEE International Conference on Robotics and Automation (IEEE Cat. No. 04ch37508)* (pp. 284–289).

Lu, X., & Xing, Z. (2022). Application of IoT quadrotor dynamics simulation. *Electronics*, *11*(4), 590. https://doi.org/10.3390/electronics11040590

Ofodile, N. A., & Turner, M. C. (2016). Decentralized approaches to anti-windup design with application to quadrotor unmanned aerial vehicles. *IEEE Transactions on Control Systems Technology*, *24*(6), 1980–1992. https://doi.org/10.1109/TCST.2016.2521799

Ofodile, N. A., & Turner, M. C. (2017). Anti-windup design for input-coupled double integrator systems with application to quadrotor UAV's. *European Journal of Control*, *38*, 22–31. https://doi.org/10.1016/j.ejcon.2017.07.002

Ofodile, N. A., Turner, M. C., & Ubadike, O. C. (2015). Channel-by-channel anti-windup design for a class of multivariable systems. In *2015 American Control Conference (ACC)* (pp. 2045–2050).

Richards, C. M., & Turner, M. C. (2020). Combined static and dynamic anti-windup compensation for quadcopters experiencing large disturbances. *Journal of Guidance, Control, and Dynamics*, *43*(4), 673–684. https://doi.org/10.2514/1.G004575

Sabour, M., Jafary, P., & Nematiyan, S. (2023). Applications and classifications of unmanned aerial vehicles: A literature review with focus on multi-rotors. *The Aeronautical Journal*, *127*(1309), 466–490. https://doi.org/10.1017/aer.2022.75

Tarbouriech, S., Garcia, G., da Silva Jr, J. M. G., & Queinnec, I. (2011). *Stability and stabilization of linear systems with saturating actuators*. Springer Science & Business Media.

Tarbouriech, S., & Turner, M. (2009). Anti-windup design: An overview of some recent advances and open problems. *IET Control Theory & Applications*, *3*(1), 1–19. https://doi.org/10.1049/iet-cta:20070435

Tseng, C. S., Chen, B. S., & Uang, H. J. (2001). Fuzzy tracking control design for nonlinear dynamic systems via TS fuzzy model. *IEEE Transactions on Fuzzy Systems*, *9*(3), 381–392. https://doi.org/10.1109/91.928735

Turner, M. C., Herrmann, G., & Postlethwaite, I. (2007). Incorporating robustness requirements into antiwindup design. *IEEE Transactions on Automatic Control*, *52*(10), 1842–1855. https://doi.org/10.1109/TAC.2007.906185

Yang, L., Li, B., Li, W., Brand, H., Jiang, B., & Xiao, J. (2020). Concrete defects inspection and 3D mapping using CityFlyer quadrotor robot. *IEEE/CAA Journal of Automatica Sinica*, *7*(4), 991–1002. https://doi.org/10.1109/JAS.2020.1003234

Zaccarian, L., & Teel, A. R. (2011). *Modern anti-windup synthesis: Control augmentation for actuator saturation* (Vol. 36). Princeton University Press.